

Blue emitting pentacoordinated Al(III) complexes based on 2-methylquinolin-8-olate and substituted phenolate ligands. The role of phenolate derivatives on emission and absorption properties†

Massimo La Deda,^a Iolinda Aiello,^a Annarita Grisolia,^b Mauro Ghedini,^{*a} Mario Amati^b and Francesco Lelj^{*b}

Received 21st July 2005, Accepted 7th September 2005

First published as an Advance Article on the web 7th November 2005

DOI: 10.1039/b510463g

This paper reports the synthesis, characterisation and photophysical investigation of the homologous series of blue-emitting pentacoordinated AlQ_2L complexes **1–6**, where Q' is 2-methylquinolin-8-olate and L is a phenolate substituted in para to the oxygen donor atom. Both electron attracting and electron releasing substituents have been considered. Also binuclear complexes of formula $\text{Q}'_2\text{Al-L}'\text{-AlQ}'_2$, where $\text{L}' = \text{OC}_6\text{H}_4\text{C}_6\text{H}_4\text{O}$, $\text{OC}_6\text{H}_4(\text{CH}_2)_3\text{C}_6\text{H}_4\text{O}$ and $\text{OC}_6\text{H}_4\text{C}(\text{CH}_3)_2\text{C}_6\text{H}_4\text{C}(\text{CH}_3)_2\text{C}_6\text{H}_4\text{O}$ have been synthesised and characterised. These are interesting blue-emitting materials for OLED (organic light emitting diode) fabrication. A comparison between computational and experimental results allowed the description of the absorption and fluorescence processes. A study of the frontier orbitals involved in the electric conduction and fluorescence emission has been performed. Influences of the phenolate-based ligands on the compounds spectroscopy have been particularly taken into account.

Introduction

The future of organic light emitting diodes (OLEDs) is certainly bound to their application in the technology of flat full-colour displays. In this sense, tuning the peak wavelength of the emitted light through chemical structure design is an important and challenging goal. Aluminium tris(quinolin-8-olate) (AlQ_3) is by far the most studied compound for OLEDs fabrication. It finds application in the so-called molecular OLEDs. These are OLEDs based on relatively low molecular weight molecules with weak intermolecular interactions in the solid phase. In fact, the emission properties of AlQ_3 can be associated to intramolecular deactivating processes (the exciton can be localised on a single molecule). Furthermore, AlQ_3 electric conduction is accurately described as an electron hopping between neighbouring molecules rather than the result of extensive electron delocalization in the solid phase. For this reason, numerous theoretical researches succeeded in understanding many phenomena occurring in AlQ_3 solid phase although they have been applied to a single molecule in vacuum.^{1a–e} Density functional theory (DFT) has been used to study the interaction between AlQ_3 and metallic atoms with the aim to model typical processes of the electrode– AlQ_3 interface.^{1f} Configuration interaction (CI) techniques, combined with DFT

and time dependent DFT (TD-DFT), have been applied to describe the emission process in AlQ_3 .^{1g}

AlQ_3 presents several desirable properties for OLED fabrication, among which the stability of amorphous AlQ_3 films (thermal stability, resistance to crystallisation, relatively long life under voltage application) and good electroluminescence properties, as well as low cost and easy processability during OLED fabrication.² However, one of its drawbacks is the electroluminescence maximum at about 520 nm, in the green region of the spectrum. This limits its applications in full-colour displays, which is the principal demand of the market. For such displays, efficient emission in the three primary colours spectral ranges (red, green and blue) is needed. Efficient green and red emission can be obtained with pure AlQ_3 and AlQ_3 doped with dyes, respectively.³ However, the blue component (between 430 and 500 nm) of the AlQ_3 electroluminescence band amounts to only about the 16% of the total.⁴ Therefore, even the inclusion of very efficient blue dyes in an AlQ_3 matrix does not produce an efficient blue-OLED. Host materials with emission peak under 500 nm are necessary for efficient emission in the blue range. Thus, efforts have been aimed to shift the luminance of AlQ_3 to the blue region by, for example, introducing donors at positions 2 or 4, or acceptors at position 5 or 7 of the 8-hydroxyquinoline ligand.⁵ Aluminium tris(4-methylquinolin-8-olato), although blue shifted with respect to AlQ_3 , emits at about 515 nm, and therefore it is still unsuitable for use as a blue emitter for display purposes.⁶

Possible candidates for replacing AlQ_3 in blue-emitting devices are pentacoordinated aluminium complexes, $\text{AlQ}'_2\text{L}$ which contain two molecules of chelant 2-methylquinolin-8-olate, Q' in the following, and a monodentate ligand, L in the following.⁷ Promising HL ligands could be phenol and substituted phenols. In fact, several phenolate-based $\text{AlQ}'_2\text{L}$ complexes exhibit sufficient stability and useful efficiency as blue-emitting materials in double-layered OLEDs.⁸ However, despite their useful properties, few studies have addressed to the origin of the blue-shifted emission

^aCentro di Eccellenza CEMIF.CAL-LASCAMM, CR-INSTM Unità della Calabria, Dipartimento di Chimica, Università della Calabria, I-87036, Arcavacata di Rende(CS), Italy. E-mail: m.ghedini@unical.it; Fax: +39 (0)984 492066; Tel: +39 (0)984 492062

^bLASCAMM, CR-INSTM Unità della Basilicata and LaMI, Dipartimento di Chimica, Università della Basilicata, I-85100, Potenza, Italy. E-mail: lelj@unibas.it; Tel: +39 (0)971 202246

† Electronic supplementary information (ESI) available: Synthesis details of complexes **1–6**, computed geometry of compounds **A**, **B**, **2–4**, computed excited states energy of compounds **A**, **B**, **2–4**, parameters of the Gaussian curves obtained from decomposition of the fluorescence emission spectra of complexes **1–4** in solution and in KBr pellets, fluorescence emission spectrum of $\text{Q}'_2\text{Al}(\mu\text{-O})\text{Q}'_2\text{Al}$ in solution. See <http://dx.doi.org/10.1039/b510463g>

in this new class of luminescent compounds, although some authors attribute it to the relative weakness of the metal–nitrogen bond.^{7d} Furthermore, the role of the phenolate ligand has not been sufficiently treated.

This paper reports on the synthesis, characterisation, photo-physical investigation and computational studies of the homologous series of blue-emitting pentacoordinated $\text{AlQ}'_2\text{L}$ complexes **1–6** shown in Chart 1. The aim of the present study is to clarify the role of the pentacoordination on the emissive properties of aluminium quinolin-8-olates. Additionally, particular interest has been addressed to the influences of the HL ligand on the complex spectroscopic features; therefore, electron-donating (in **1**, **4**, **5** and **6**) and electron-withdrawing (in **2** and **3**) substituents were selected and the possibility of producing tunable luminescent $\text{AlQ}'_2\text{L}$ molecules was investigated. Moreover, considering that a useful material for OLED application should have good charge carrier mobility, and that charge transport can be enhanced by linking two metal centres,^{3f} two classes of compounds were synthesised: mononuclear (**1–3**) and binuclear (**4–6**) aluminium complexes. In this way, it was possible to explore the effects of the interaction between the AlQ'_2 emitting fragments when they are joined by aromatic rings (**4**) or by aromatic rings connected through an

aliphatic chain (**5**, **6**). The computational study was performed on complexes **2–4** and on two model compounds, **A** (with $\text{L} = \text{OC}_6\text{H}_5$) and **B** (with $\text{L} = \text{OC}_6\text{H}_4\text{CH}_3$).

Results and discussion

Synthesis

For the synthesis of complexes **1–6**, aluminium isopropoxide was reacted by adapting procedures developed for the preparation of similar complexes.^{7b} In particular, the mononuclear complexes **1–3** were synthesised reacting aluminium isopropoxide with the appropriate phenol and 2-methyl-8-hydroxyquinoline in a ratio 1 : 1 : 2, in toluene. The binuclear complexes **4–6** were prepared by reacting two molar equivalents of the aluminium isopropoxide in the presence of one molar equivalent of the appropriate bis-phenol and four molar equivalents of 2-methyl-8-hydroxyquinoline. All the new complexes were obtained in good yields and were yellowish solids, exhibiting the expected stoichiometry (see ESI†) in the elemental analyses. Moreover, these compounds were characterised by IR and, in the case of complex **1** which was well soluble in dichloromethane, ¹H NMR spectroscopic

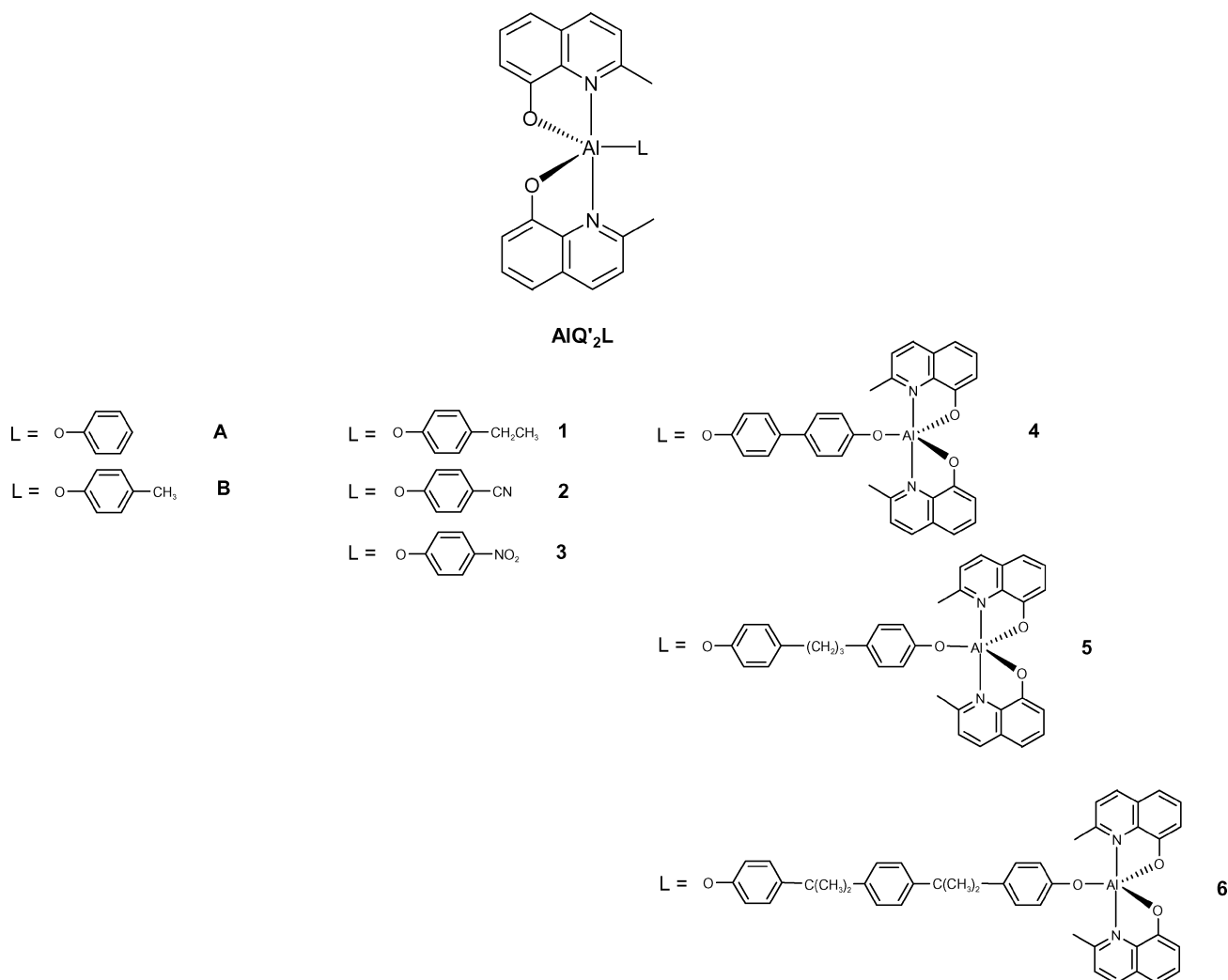


Chart 1 Molecular structures of synthesised complexes **1–6** and the model complexes **A** and **B**.

characterisation was also carried out (see ESI†). According to the X-ray crystal structure reported for the isobutylbis(2-methylquinolin-8-olate)aluminium complex, Q_2Al^iBu ,⁹ in the homologous series of pentacoordinated complexes **1–6** described in the present study, the aluminium coordination polyhedron can be considered a distorted trigonal bipyramid, in which four sites are taken up by two bidentate *Q* ligands, and the fifth one filled by the monodentate phenoxide ligand.

Photophysical measurements

The photophysical data are collected in Table 1; the reported relative luminescence intensities in solution were evaluated from the area of the luminescence spectra with reference to a luminescence standard $[Ru(bpy)_3]Cl_2$ ($\Phi = 0.028$ in air-equilibrated water¹⁰).

Reference to electronic spectra of similar compounds⁷ suggests that the absorption and emission bands (Fig. 1 and 2) can be assigned to transitions localised on the *Q* ligands. In fact, no appreciable differences were observed when the spectra were compared among these complexes and with those of similar compounds.^{7b} Furthermore, these complexes show a relevant blue-shifted emission with respect to AlQ_3 , whereas the luminescence quantum yield remains of the same order of magnitude.¹¹

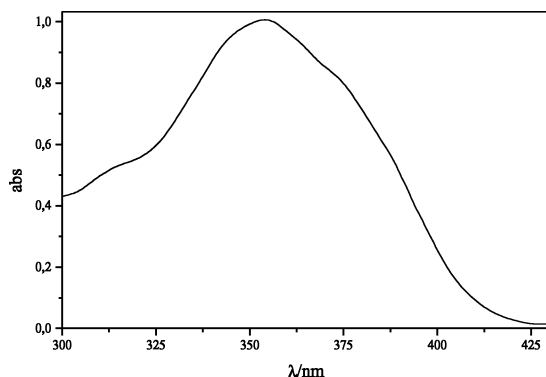


Fig. 1 Absorption spectrum of the complex **4** in dichloromethane solution.

The AlQ_2L complexes exhibited different spectral features in CH_2Cl_2 solution and in solid phase, suggesting that the *L* fragment affects the intermolecular interactions. In particular, the emission band of the solid samples spectra of **1**, **3** and **6** are ipsochromically shifted with respect to their solutions spectra, while compounds **2**, **4** and **5** are bathochromically shifted (Table 1).

Table 1 Photophysical data of synthesised complexes **1–6**

Compound	Solution (CH_2Cl_2)		Solid (KBr pellets)	
	Abs./nm	Em./nm	Abs./nm	Em./nm
1	260, 354	490 (14%)	260, 390	460
2	260, 354	480 ^a	260, 360	490
3	260, 356	480 ^a	278, 400	468
4	260, 356	480 (10%)	260, 360	488
5	260, 352	490 (7%)	260, 360	480
6	260, 358	480 (11%)	260, 360	476

^a Low solubility of the complexes prevents accurate quantum emission yield determination which was in the order of 10–15%.

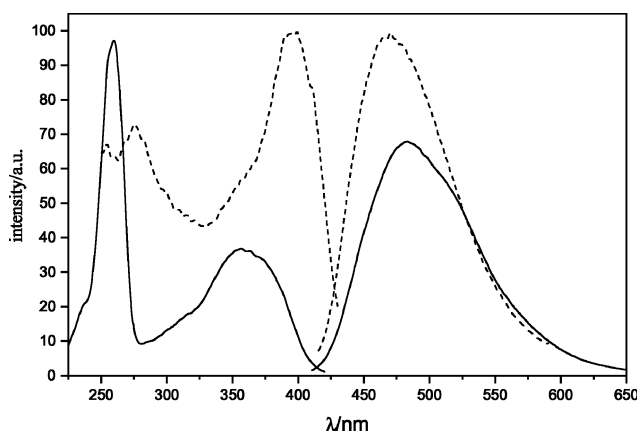


Fig. 2 Excitation (on the left; $\lambda_{em} = 475$ nm) and emission (on the right; $\lambda_{ex} = 375$ nm) spectra of **3** in solution (solid line) and in solid (dashed line).

The negligible effect that the various *L* fragments have on absorption and emission spectra in solution could be accounted for by low perturbations exerted by the phenolate molecular orbitals on the *Q* chelants. Furthermore, no differences have been recorded in the electronic spectra of the binuclear compounds (**4–6**). This excludes relevant electronic effects that could be attributed to two metal centres interactions, mediated through delocalised electrons (**4**) or through space (**5** and **6**).

To clarify these crucial points a computational study has been performed on the synthesised complexes **2**, **3** and **4** and on two model complexes **A** and **B**. Compound **A** has to be considered a parent molecule for a general description of the ground and excited states characteristics. Compound **B** has been used in place of compound **1** for simplifying the geometry optimisation. It is reasonable that substantially equivalent perturbations are induced by the methyl and ethyl groups.

Computational study of model compound A

The computed geometry of **A** is shown in Fig. 3 and Table 2 presents some computed geometrical parameters compared with the computed ones for the *mer*- AlQ_3 isomer^{1c,e} (*mer*- AlQ_3 is the most stable AlQ_3 isomer in solution). The complete geometry is reported in ESI (Table S1†).

Table 2 Selected bond lengths computed at the B3LYP/6-31G(d) level of approximation for the complex **A**. The computed values of *mer*- AlQ_3 are reported for comparison

Compound	Bond	Length/Å
A	Al–O1	1.764
	Al–O2	1.820
	Al–O3	1.820
	Al–N1	2.076
	Al–N2	2.087
<i>mer</i> AlQ_3	Al–O	1.881
		1.884
		1.885
	Al–N	2.125
		2.064
	2.084	

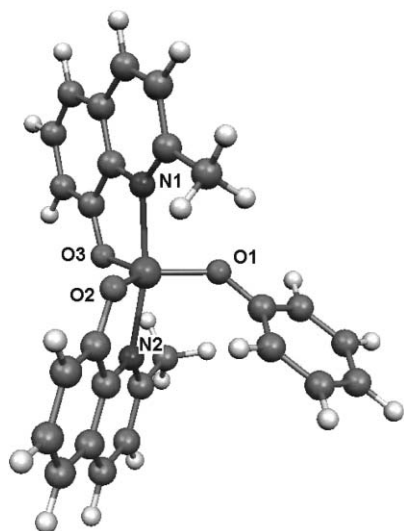


Fig. 3 The computed structure of the model complex **A**. The atoms of the coordination sphere are labelled for reference in Table 2.

As shown in Table 2, the Al–O bond distances of **A** are shorter when compared to those of AlQ_3 ; in fact the Al–O bond distances associated with the Q' chelants are shorter by at least 0.061 Å. The Al–N distances of **A** are comparable to the two shortest Al–N distances of AlQ_3 . If the longest Al–N distance of AlQ_3 (2.125 Å) is not considered, the maximum difference between the Al–N bond distances of **A** and AlQ_3 is 0.023 Å. If we consider that the Al–N distances are longer than the Al–O distances, it is clear that the Al–O bonds experience the largest percentage change in **A** when compared to AlQ_3 . This point will be discussed below when considering the origin of the blue-shift in the emission spectra of AlQ_2L complexes.

Fig. 4 shows the Kohn–Sham orbitals of **A** whose energy levels are close to that of the HOMO (the highest-in-energy occupied molecular orbital) and the LUMO (the lowest-in-energy unoccupied molecular orbital). It is worthy to note that all the

reported orbitals have negligible contributions from the central metal orbitals. This feature has also been observed in AlQ_3 .¹ Interestingly, the HOMO is localised on the phenolate ligand, whereas the LUMO is localised on the quinolate moieties. Fig. 4 also shows the Kohn–Sham orbital energy levels used for assigning the absorption and emission bands of **A**. The associated orbitals can be grouped in orbitals which are localised on the phenolate fragment and those localised on the Q' fragments. Furthermore, each Kohn–Sham orbital of the isolated and negatively-charged ligand (referred to as fragment orbital). They are shown in Fig. 4. The occupied orbitals 114 (HOMO), 111 and 108 and the virtual orbitals 119 and 122 are localised on the phenolate moiety, while the remaining orbitals are localised on the Q' chelants and form couples of almost degenerate orbitals: couples 106–107, 109–110, 112–113 of occupied orbitals, couples 115–116, 117–118, 120–121 of virtual orbitals. These orbitals are mainly delocalised on the two Q' rings, but the fragment orbitals from which these are composed interact weakly and exhibit similar energy (calculated from the expectation value of the Kohn–Sham operator). Thus, the delocalization of the resulting almost degenerate couple of orbitals should not be interpreted as the consequence of relevant electronic interactions.

The energies of the orbitals shown in Fig. 4 and their classification as quinolate (q' label) or phenolate localised orbital (ph label) are listed in Table 3. The HOMO–LUMO energy gap in **A** is larger when compared to that in AlQ_3 (3.60 vs. 3.27 eV^{1e}).

Table 4 reports the principal excited states, their oscillator strengths and composition in terms of Kohn–Sham orbitals (mono-electron excitations). It is apparent that the computed absorption spectrum is dominated by two transitions at 391 and 240 nm, with the second one being much more intense. Interestingly, these two absorptions are mainly associated to q' orbitals. Furthermore, close to the intense transition at 240 nm, two transitions at 245 and 244 nm were computed. As illustrated in Table 4, they receive a larger contribution from the ph orbitals.

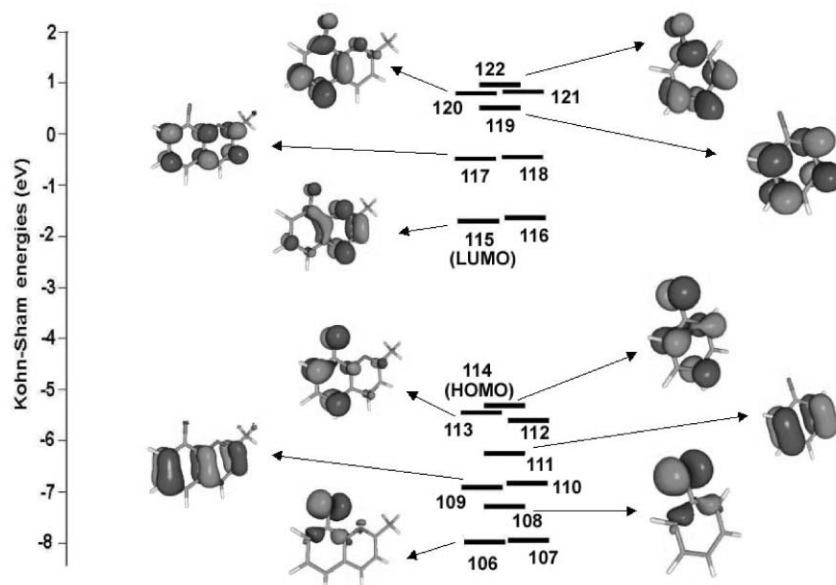


Fig. 4 The energy scheme of the Kohn–Sham orbitals computed for the complex **A**. The fragment orbitals with larger contribution have been reported.

Table 3 One-electron energies and composition of the highest occupied and the lowest unoccupied Kohn–Sham orbitals of **A**. The phenolate-localised orbitals (*ph*) and the couple of almost degenerate orbitals localised on the 2-methylquinolin-8-olate (*q'*) moieties have been labelled for easiest reference in the following. The fragment orbitals and their energy levels are shown in Fig. 4. B3LYP/6-31G(d) level of approximation

Label	Orbital	Energy/eV	MO main composition
<i>q'1</i>	106	-7.95056	2-Methylquinolin-8-olate
	107	-7.91166	2-Methylquinolin-8-olate
<i>ph1</i>	108	-7.29776	Phenolate
<i>q'2</i>	109	-6.84869	2-Methylquinolin-8-olate
	110	-6.83373	2-Methylquinolin-8-olate
<i>ph2</i>	111	-6.25246	Phenolate
<i>q'3</i>	112	-5.63883	2-Methylquinolin-8-olate
	113	-5.4536	2-Methylquinolin-8-olate
<i>ph3</i> (HOMO)	114 (HOMO)	-5.31107	Phenolate
<i>q'4</i> (LUMO)	115 (LUMO)	-1.71496	2-Methylquinolin-8-olate
	116	-1.64696	2-Methylquinolin-8-olate
<i>q'5</i>	117	-0.4945	2-Methylquinolin-8-olate
	118	-0.46131	2-Methylquinolin-8-olate
<i>ph4</i>	119	0.51136	Phenolate
<i>q'6</i>	120	0.769216	2-Methylquinolin-8-olate
	121	0.804032	2-Methylquinolin-8-olate
<i>ph5</i>	122	0.952544	Phenolate

From the above analysis, it is possible to conclude that the absorption spectrum calculated for **A** is dominated by transitions between orbitals belonging to the Q' chelants. Very interestingly, S₁ and S₂ singlet states (Table 4) are mainly associated to charge-transfer transitions between L-localised occupied orbitals (*ph3* orbitals) and Q'-localised unoccupied orbitals (*q'4* orbitals). In the following paragraph, compounds **B**, **2**, **3** and **4** will be compared to the parent compound **A**, with the aim to underline differences induced by the substituents on the phenolate ligand.

Table 4 B3LYP/6-31G(d) singlet–singlet excitation energies (eV and nm), oscillator strengths (*f*) and composition of the excited state-function (threshold of reported coefficients = 0.001) for the complex **A**. Only transitions with oscillator strength higher than 0.01 are reported for excitation 7 and the successive ones. The complete list of excitations is reported in Table S2 (ESI†)

Excited state	Composition	Energy/eV (wavelength/nm)	<i>f</i>
S ₁	<i>ph3</i> → <i>q'4</i> ; 0.50 (HOMO–LUMO)	3.01 (412)	0.0004
S ₂	<i>ph3</i> → <i>q'4</i> ; 0.43	3.12 (398)	0.0098
	<i>q'3</i> → <i>q'4</i> ; 0.05		
S ₃	<i>q'3</i> → <i>q'4</i> ; 0.40	3.17 (391)	0.0738
	<i>ph3</i> → <i>q'4</i> ; 0.05		
S ₄	<i>q'3</i> → <i>q'4</i> ; 0.44	3.25 (382)	0.0047
S ₅	<i>q'3</i> → <i>q'4</i> ; 0.47	3.39 (366)	0.0019
S ₆	<i>q'3</i> → <i>q'4</i> ; 0.47	3.44 (360)	0.0058
S ₁₄	<i>q'3</i> → <i>q'5</i> ; 0.48	4.63 (268)	0.0062
	<i>q'2</i> → <i>q'4</i> ; 0.01		
	<i>q'2</i> → <i>q'4</i> ; 0.14		
	<i>ph2</i> → <i>ph5</i> ; 0.03	5.07 (245)	0.1193
S ₂₀	<i>q'3</i> → <i>q'5</i> ; 0.09		
	<i>ph3</i> → <i>ph4</i> ; 0.12		
	<i>q'2</i> → <i>q'4</i> ; 0.07		
	<i>ph2</i> → <i>ph5</i> ; 0.06	5.09 (244)	0.1159
S ₂₁	<i>q'3</i> → <i>q'5</i> ; 0.05		
	<i>ph3</i> → <i>ph4</i> ; 0.24		
	<i>q'1</i> → <i>q'5</i> ; 0.01		
	<i>q'2</i> → <i>q'4</i> ; 0.19	5.16 (240)	0.7270
	<i>q'3</i> → <i>q'5</i> ; 0.14		
	<i>ph3</i> → <i>ph4</i> ; 0.02		

^a The molecular orbitals are labelled according to Table 3.

Computational study of the compounds **B**, **2**, **3** and **4**

DFT and TD-DFT computations were performed on the **B**, **2**, **3** and **4** compounds. The geometrical structures were optimised at the B3LYP/6-31G(d) level of approximation. The complete structures of **B**, **2**, **3** and **4** are presented in Table S1 (see ESI†). They all result to be asymmetric.

Information regarding the frontier orbitals of these compounds is presented in Table 5, with the orbitals ordered according to their energy and, when possible, labelled as in Table 3. In the case of **2** the HOMO–1 and HOMO–2 are delocalised on L (Chart 1) and Q' ligands, whereas in the case of the binuclear complex **4**, which contains four Q' chelants, four almost degenerate orbitals are localised on Q'.

From Table 5, it is possible to verify that, in comparison to the complex **A**, the CN and NO₂ electron withdrawing groups (compounds **2** and **3**) lower (make more negative) the energy of the L-localised orbital *ph3*. Consequently, the HOMO becomes localised on the Q' chelants. Orbitals *q'3* and *q'4* are weakly affected by the substituent carried by the L ligand and the energy gap between them is the same of **A** (3.74 eV). As a consequence, the HOMO–LUMO gap increases from 3.60 eV (in **A**) to 3.74 eV (in **2** and **3**). On the contrary, the presence of electron-donating groups (in **4** and **B**) destabilises of the *ph3* HOMO, reducing the HOMO–LUMO energy gap to 3.34 eV (complex **B**) and to 2.85 eV (binuclear complex **4**); interestingly, the energy gaps between *q'3* and *q'4* in **B** and **4** are practically the same as **A** (3.74 eV). Some relevant computed electronic transitions up to the most intense absorption around 240 nm are presented in Table 6.

The case of the complex **A** has been reported for comparison. It is possible to note that the first intense absorption band falls at about 392 nm in all the compounds. This transition principally consists in the *q'3*–*q'4* excitation (Table 4), thus it is associated to

Table 5 The Kohn–Sham orbital energies (eV) and the HOMO–LUMO gaps (eV) of **2**, **3**, **4**, **A** and **B**. The orbitals have been labelled according to Table 3, where possible

2	3	4	A	B
–1.88 (<i>q'4</i>)	–1.92 (<i>q'4</i>)	–1.60 (<i>q'4</i>) –1.60 (<i>q'4</i>) –1.67 (<i>q'4</i>)	–1.65 (<i>q'4</i>)	–1.64 (<i>q'4</i>)
–1.95 (<i>q'4</i>) ^a	–1.99 (<i>q'4</i>) ^a	–1.67 (<i>q'4</i>) ^a	–1.71 (<i>q'4</i>) ^a	–1.72 (<i>q'4</i>) ^a
–5.69 ^{b,c}	–5.73 (<i>q'3</i>) ^b	–4.52 (<i>ph3</i>) ^b	–5.31 (<i>ph3</i>) ^b	–5.06 (<i>ph3</i>) ^b
–5.84 ^d	–5.91 (<i>q'3</i>)	–5.40 (<i>q'3</i>) –5.40 (<i>q'3</i>)	–5.45 (<i>q'3</i>)	–5.46 (<i>q'3</i>)
–5.89 ^d	–6.11 (<i>ph3</i>)	–5.59 (<i>q'3</i>) –5.59 (<i>q'3</i>)	–5.64 (<i>q'3</i>)	–5.64 (<i>q'3</i>)
3.74 ^e	3.74 ^e	2.85 ^e	3.60 ^e	3.34 ^e
3.74 ^f	3.74 ^f	3.74 ^f	3.74 ^f	3.74 ^f

^a LUMO. ^b HOMO. ^c Orbital localised on the two Q' chelants. ^d Orbitals delocalised on both Q' and L. ^e HOMO–LUMO energy gap. ^f *q'3*–*q'4* energy gap.

Table 6 The most important electronic transitions (nm) computed for the series of compounds **2**, **3**, **4**, **A** and **B**. A threshold of 0.01 has been used for the reported oscillator strength (in parenthesis). Given the large size of the molecule, for the complex **4** only the first 26 excited states have been computed. They correspond to the first absorption band

2	3	4	A	B
392 (0.08)	392 (0.08)	392 (0.17)	398 (0.01)	392 (0.08)
356 (0.01)	383 (0.01)	383 (0.02)	391 (0.07)	360 (0.01)
267 (0.01)	338 (0.01)	361 (0.01)	360 (0.01)	268 (0.01)
253 (0.01)	301 (0.39)		268 (0.01)	250 (0.01)
245 (0.44)	266 (0.01)		245 (0.12)	249 (0.01)
	253 (0.01)		244 (0.12)	245 (0.22)
	246 (0.01)		240 (0.73)	240 (0.69)
	245 (0.05)			
	244 (0.15)			
	240 (0.67)			

the Q' chelants. As seen before, the energy gaps between occupied and virtual orbitals localised on Q' do not change in the series of studied compounds, and this could be reflected in the invariance of the predicted first absorption. The computed transition at 392 nm is followed at shorter wavelengths by the most intense band, predicted at 240 nm in all the cases, apart from **2** where it is computed at 245 nm. The latter transition is mainly localised on the Q' chelants and it is equivalent to the transition associated to the state S₂₁ in the case of **A** (Table 4). Other transitions of significant oscillator strengths have been computed close to the most intense band, at slightly longer wavelengths. It is reasonable to suppose that such bands are not easily seen in the experimental spectra because they could be too close to the most intense band.

Hence, the computations describe the presence of two significant features, one at longer wavelength (392 nm) and one, more intense, at about 240 nm. This is true for all the compounds but **3** for which an intense band at 301 nm is computed. It can be assigned to the mono-electronic excitation from the *ph3* orbital to a π* orbitals mostly localised on the NO₂ group.

Comparison with the experimental spectra

The computational description of the previous paragraphs well agrees with the experimental spectra. The substantial invariance of the experimental absorption spectra among the studied complexes

has been discussed in precedence. The experimental spectra of **1**, **2** and **4** show two principal features at about 355 and 260 nm irrespective of the withdrawing and releasing properties of the substituents on the phenolate moiety (Table 1).

The good agreement between computed and experimental absorption spectra allows to describe with good confidence the main absorption processes. Furthermore, it gives suggestions about the excited states kinetic after light absorption. Table S3 (see ESI†) collects more detailed information about the lowest-energy excited states which are associated to the first absorption band and are involved in emission of light. As said before, on the basis of computed oscillator strengths and experimental analysis, light absorption mostly involves transitions associated to the Q' chelants. Absorption mostly leads to the first singlet excited state in the case of electron-withdrawing groups (R = CN and NO₂ in **2** and **3**, respectively). In these cases, we can expect that also the emission process takes place from the same excited state, in other words, both absorption and emission are processes mostly involving the Q' chelants, and in particular the lowest excited state S₁. The other compounds seem to be different. **A**, **B** and **4** absorption mostly leads to the lowest-energy excited state which involves orbitals localised in the Q' chelants, that is S₃ for **A** and **B**, and S₅ in the case of **4**, owing to their larger oscillator strengths. Thus, after absorption, there are in principle two deactivation paths. The first one is the occurrence of internal conversion with consequent population of S₁ and emission from this state. If this is the case, a red-shifted emission should have been observed. The second possibility is that the rate of the internal conversion to S₁ is too low in comparison to the rate of emission from the above mentioned S₃ and S₅ singlet states. Thus, emission takes place directly from these states. Although this contradicts the Kasha principle,¹² this behaviour could be due to the almost orthogonality of fragment orbitals localised on L and Q'.

Experimental emission fluorescence data are collected in Table 1 and Fig. 2. As said above, a simple glance allows noting an unexpected similarity between the emission fluorescence spectra of the studied complexes. Only a small red shift has been detected in the case of **1** and **5**. We have analysed in a quantitative way the experimental emission spectra by decomposing their profile by three Gaussian functions. We have used a common value for their width. Fig. 5 presents a pictorial view of the results, whereas Table S4 (see ESI) lists the parameters characterising the Gaussian curves.

From Table S4† and Fig. 5, it can be noted that the four emission spectra might result from a vibronic progression of three overlapping peaks, or at least two asymmetric peaks whose tail at longer wavelengths has been described by the weakest Gaussian curve at longer wavelengths (Gaussian 3 in Table S4†). A finding to be highlighted is the high similarity in the λ_{max} of the three Gaussian curves. The largest energy difference among the studied compounds is 0.02 eV, to be compared to the HOMO–LUMO gaps reported in Table 5, whose differences fall in a range of 0.89 eV. Furthermore, the separation in energy between Gaussian 1 and Gaussian 2 curves goes from 0.24 to 0.21 eV, and the separation between Gaussian 2 and Gaussian 3 ranges from 0.20 to 0.22 eV. It can be concluded that fluorescence emission mostly involves Q' chelants, with little influence from the L ligand. As said about the similarity among absorption spectra, the weak influence

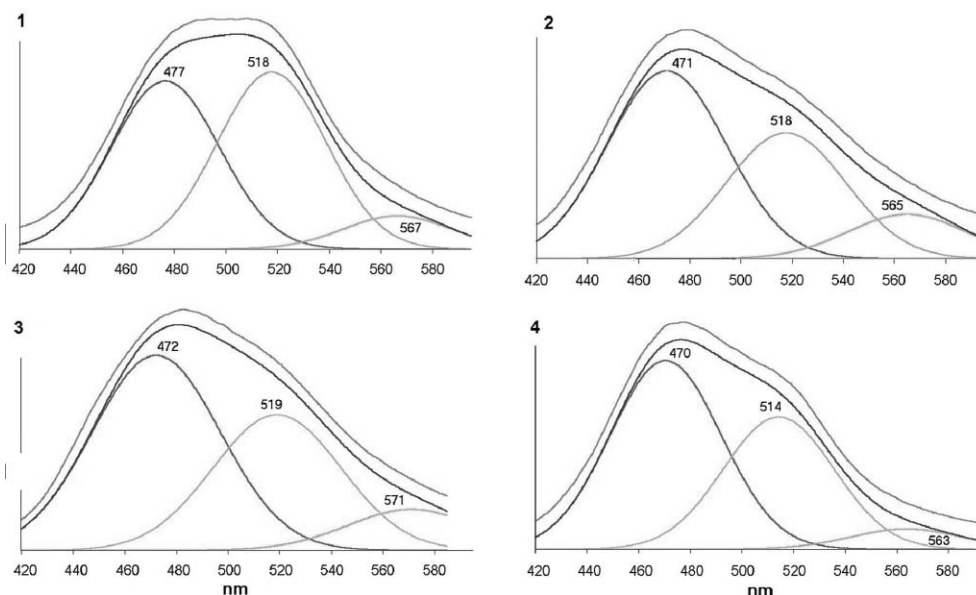


Fig. 5 Decomposition of the experimental fluorescence emission spectra for the complexes **1–4**. All the emission spectra have been recorded in CH_2Cl_2 solution, with an excitation wavelength of 355 nm. The highest curve in each graph is the experimental spectrum. The one beneath is the corresponding combination of the Gaussian curves. The experimental curve has been shifted at higher values to be distinguished from the fitted curve.

of the L ligand on the Q' -localised orbitals can be considered a good explanation of the great similarity among emission spectra.

The influence of the L ligands on the emission process has been definitely ruled out by comparing the fluorescence emission spectra of the four studied compounds with the binuclear complex $[\text{AlQ}'_2]_2(\mu\text{-O})$. This is widely described in the ESI†

Fig. 6 summarises the computational results about absorption and fluorescence emission of the four studied compounds in CH_2Cl_2 solution, considering **B** as a plausible model for **1**. The arrows between S_0 and the excited states have been reported to describe the main absorption and fluorescence emission processes. As said before, the most important absorption process for **2** and

3 takes place between S_0 and S_1 ; thus, S_1 should be considered the emitter state. For **1** and **4**, the most probable absorption leads to S_3 and S_5 excited states, respectively. In both the cases, they appear to be the most probable emissive states in fluorescence emission.

In fact, according to the computations, there are excited states at lower energy (S_1 and S_2 for **1** and S_1 , S_2 , S_3 and S_4 for **4**) which do not take part in the fluorescence process. We tried to find an experimental confirm of the existence of these low energy states, in which the L ligand plays an important role. This investigation has been performed on complex **4**. Fig. 7(a), shows a portion of the emission fluorescence spectra recorded at an excitation wavelength of 355 nm.

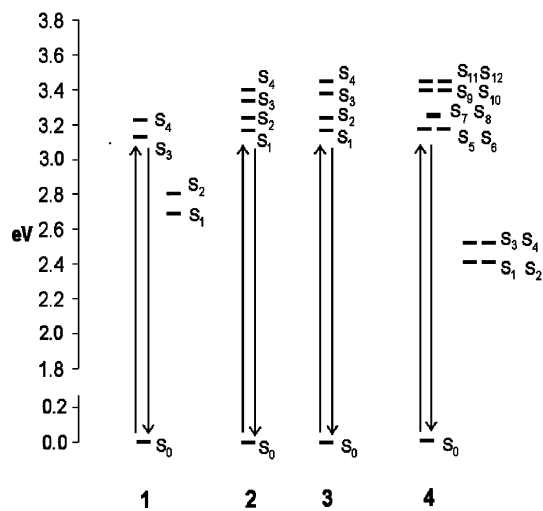


Fig. 6 Level scheme of the computed ground and excited states in the series of studied compounds. The most important absorption and emission transitions are represented by arrows.

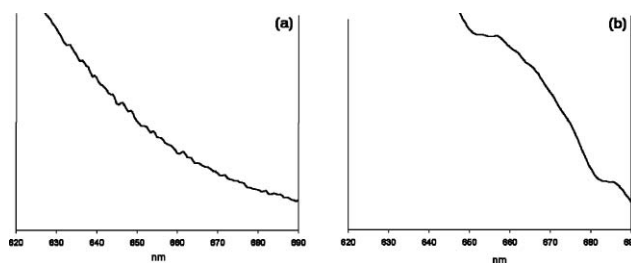


Fig. 7 Fluorescence emission spectra of **4** obtained by exciting at 355 nm (a) and 490 nm (b) in CH_2Cl_2 solution.

This corresponds to the maximum of the first absorption band, which can be assigned to Q' localised electronic transitions. Fig. 7(b) shows the same portion of the emission spectra when an excitation wavelength of 490 nm was used. At this wavelength, absorption from Q' is far less intense and, according to the computations, in this zone of the spectrum weak absorption bands should exist for excitations toward excited states in the range from S_1 to S_4 (Table S3, ESI†). In this case, at about 660 nm, a weak

emission peak has been detected. This is shifted of about 0.70 eV in comparison to the emission peak exciting at 355 nm (emission from Q' chelants at 480 nm). This energy shift is to be compared with the computed 0.77 eV energy difference between the computed HOMO–LUMO gap and the energy gap between occupied and virtual orbitals on Q' chelants (2.85 and 3.74 eV, as reported in Table 5). Furthermore, the LUMO orbital is an anti-bond orbital, whereas the highest occupied orbitals, both on L and on Q', are substantially non-bonding. Thus, it can be predicted that the largest part of the geometry relaxation of the excited state is due to geometry deformations of Q', with probable changes in the coordination sphere as a consequence of charge transfers between ligands, a phenomenon suggested for AlQ₃.^{1g} Given the nature of the metal–ligand interaction in this class of compound, which is essentially electrostatic, the deformation of the Q' chelants may be predicted to contribute significantly to the energy stabilisation. Hence, a similar energy stabilisation for the lower energy excited states can be expected, irrespective of the contribution of the L ligand.

Now we are in the position to give some suggestions about the origin of the blue shift in the absorption and emission processes of the studied pentacoordinated complexes. We know that these processes should be associated to the highest occupied and the lowest unoccupied orbitals localised on the Q' chelants. These are the *q*'3 and *q*'4 orbitals of Table 3, respectively. The *q*'3 energy of A is –5.45 eV. The corresponding orbital of AlQ₃ (the HOMO) has been computed at –5.00 eV at the same level of computation.^{1e} The *q*'4 orbital is associated to an energy of –1.71 eV, to be compared to the –1.73 eV of the AlQ₃ LUMO.^{1e} It is clear that the *q*'3 orbital is more stable in comparison to the AlQ₃ HOMO, so that the energy gap between occupied and virtual orbitals on the Q' fragments increases mostly by virtue of this effect. In this respect, great emphasis should be assigned to the shortened Al–O bond distance in the five-coordinated compound (Table 2). In fact, the *q*'3 orbital shows a large contribution from the Q' oxygen donor atoms, with consequent significant energy changes associated to the Al–O bond distance variations. Thus, it seems that a correlation between geometry and blue shifted absorption and emission should be referred to the Al–O distances rather than the Al–N distances, as suggested in the literature.^{5a–7d}

An interesting point to be discussed concerns the relative intensities of the three Gaussian curves used for the spectra

decomposition. Actually, the integral of the emission band located under 500 nm determines the fraction of the emission spectrum in the range of wavelengths associated to the blue colour. This fraction amounts to 48, 55, 55 and 60%, respectively for **1**, **2**, **3** and **4**. In general, in CH₂Cl₂ solutions, the higher is the intensity of the first Gaussian curve, the higher the percentage of the emission spectrum in the blue-colour region, that is, more saturated is the emitted blue light. From the above values, and from the spectra decomposition (Table S4, ESI† and Fig. 5), it is not possible to find a simple correlation between the percentage emission in the blue region and the nature of the monodentate ligand in the structure. In fact, the complex bearing the strongest electron-donating L ligand (**4**) shows a fluorescence emission spectrum which is more similar to the cases of the complexes with the electron-withdrawing groups (**2** and **3**) rather than the cases of complexes with the weaker electron-donating L ligand (model compound **B**).

Emission spectra in solid phase

Packing effects in solid phase can change the characteristics of the emission spectra in comparison to solution phases. The different intermolecular interactions can change the nature of the electronic states, and consequently the characteristics of the absorption and emission bands, such as absorption and emission peak wavelengths, absorption intensity, emission quantum yield and band shape. A study about emission from solid phases gains particular importance when the object of the research is materials for OLEDs fabrication. Furthermore, a comparison between solution and solid phase emission can outline the environmental influences on the electronic transitions. In this light, complexes **1** and **4** are particularly interesting; the lower energy excited states, which do not seem to take part to electronic transitions (both absorption and emission) in solution phase, could become more effective in solid phase, with consequent neat change in emission properties.

The emission fluorescence spectra of the same set of compounds in solid phase have been reproduced in Fig. S4 (see ESI†). Also in this case, a decomposition based on three Gaussian curves of identical broadness has been performed and shown in Fig. S4 (ESI†). Furthermore, only three Gaussian curves were used and their parameters are reported in Table 7. In the same table, we

Table 7 Results from the decomposition of fluorescence spectra in solid phase of **1**, **2**, **3** and **4**. The spectra and their decomposition are displayed in Fig. S4 (see ESI†). Each curve is described in terms of λ_{\max} , relative intensity and full width at half maximum (FWHM). The collected data deal with solid samples in KBr pellets, and the shifts relative to the CH₂Cl₂ solutions (Table S4, ESI†) are reported in parentheses

		1	2	3	4
Gaussian 1	λ_{\max}	454 nm (–23); 2.73 eV (+0.13)	472 nm (+1); 2.63 eV (0.00)	463 nm (–9); 2.68 eV (+0.06)	470 nm (0); 2.63 eV (0.00)
	Relative I_{\max}	4.09 (–0.96)	2.70 (–1.53)	4.59 (–0.18)	6.18 (–3.83)
	FWHM/nm	55.6 (+6.2)	61.2 (+4.2)	55.6 (–3.0)	54.0 (+3.2)
Gaussian 2	λ_{\max}	486 nm (–32); 2.55 eV (+0.16)	517 nm (–0.1); 2.39 eV (–0.01)	505 nm (–14); 2.45 eV (+0.06)	513 nm (–2); 2.42 eV (+0.01)
	Relative I_{\max}	1.91 (–3.41)	2.40 (–0.44)	2.66 (–0.66)	5.83 (–1.18)
	FWHM/nm	55.6 (+6.2)	61.2 (+4.2)	55.6 (–3.0)	54.0 (+3.2)
Gaussian 3	λ_{\max}	520 nm (–47); 2.39 eV (+0.20)	562 nm (–0.03); 2.21 eV (+0.02)	552 nm (–19); 2.25 eV (+0.08)	564 nm (–1); 2.20 eV (+0.01)
	I_{\max}	1.00	1.00	1.00	1.00
	FWHM/nm	55.6 (+6.2)	61.2 (+4.2)	55.6 (–3.0)	54.0 (+3.2)

reported the differences in the same parameters in comparison to spectra recorded in CH_2Cl_2 solution.

From Fig. S4 (ESI†) and Table 7, it is evident that for **2** and **4** the position of the three Gaussian curves remains almost the same as in solutions, whereas a blue-shift has been detected for **3** and mostly for **1**. For **2** and **4**, the relative intensities of the Gaussian 1 curve decreases more than that of the Gaussian 2 one. As a consequence, the emission spectra in solid phase appears flatter, and the fraction of the spectra at wavelengths lower than 500 nm passes from 55 and 60% in solution to 50 and 56% (for **2** and **4**, respectively). On the contrary, the Gaussian 1 curve becomes more important in comparison to solution phases in the case of **1** and **3**. This fact, together with the aforementioned blue-shift, leads to an increase of the fraction of emission under 500 nm, which are 66 and 79% to be compared with 55 and 48% in solution (for **3** and **1**, respectively). The blue-shifted emission in the case of **1** is noticeable. The worst blue-emitter in solution becomes the best one in solid phase. This is not in line with the predicted trend in HOMO–LUMO gap. However, also in the case of solid samples, it can be underlined a substantial similarity between the emission spectra of the series of compounds. Thus, it can be concluded that also in the solid phase the emission process can be assigned to Q', with a small contribution from the L ligand. In a simple mono-electronic description of the observed excitation processes, the L-localised orbitals do not play a relevant role in the emissive states. However, this does not mean that the emission spectra are not influenced by L in an absolute sense. The L ligand contributes to the percentage emission under 500 nm. This is particularly true in the solid phase, where larger differences between the emission fluorescence spectra have been found, a probable consequence of changes in molecular packing and/or intermolecular interactions induced by the substituent on the L ligands.

Conclusions

Pentacoordinated aluminium (phenolate)-bis(2-methylquinolin-8-olate) compounds are good blue emitting molecular materials easy to prepare. This characteristic is retained regardless of the electronic effects exerted by the substituents placed on the phenolate ligand, a useful trait that can be utilised, for example, to graft the AIQ₂ fragment to macromolecular systems such as polymers¹³ or properly substituted porphyrins.¹⁴

Absorption and fluorescence emission of the series of compounds **1–6** can be assigned to mono-electronic excitations on orbitals localised on Q' chelants. In this respect, it can be concluded that absorption and emission phenomena mostly involve the Q' fragment, with weak contribution from the L ligand, as has been observed both in solution and in the solid phase.

By comparing the obtained results with the data referred to the six-coordinated AIQ₃, it seems that the origin of the blue-shifted emission in pentacoordinated compounds does not arise from the lengthening of the Al–N bond, as reported elsewhere, instead it could result from the shortening of the Al–O bond lengths with consequent stabilisation of the highest energy occupied orbitals localised on the 2-methylquinolin-8-olate chelants and increased energy gap with the unoccupied orbitals.

In the case of **1** and **4** the emissive state is not the first singlet excited state, as usually postulated. Thus, it seems not possible to tune the colour of the emitted light by operating on the L ligand

with substituents which are able to perturb the phenolate-localised orbitals, because this perturbation is substantially confined on the L ligand. However, the L ligand can change the shape of the emission band in the solid phase, probably because of influences on the crystal packing. As a consequence, it could increase the percentage of emission under 500 nm, and thus the intensity of the blue emission. In this sense, this effect can be considered as a sort of indirect tuning of the emitted light. In solution phase, this indirect tuning is less effective, but still observed and sufficient to distinguish emission of **1** from that of the other complexes.

Experimental

Synthesis

The preparation of complexes **1–6** is available in detail as ESI.†

Physical measurements

The apparatus and the techniques used to check the purity of the synthesised compounds were described elsewhere.¹⁵ The photo-physical properties of the synthesised species were investigated in solution by using the equipment previously described.¹⁵

Computational methods

All the computations have been performed using the Gaussian98 package.^{16a} All geometries have been optimised using the standard Gaussian98 threshold for SCF and geometry optimisation. Kohn–Sham molecular orbital and their energies have been computed by the DFT (density functional theory)^{16b} approach using the B3LYP^{16c} hybrid exchange–correlation functional and the 6-31G(d) basis set. Analytical evaluation of the energy second derivative matrix w.r.t. Cartesian coordinates (Hessian matrix) at the same level of approximation confirmed the nature of minima of the potential energy surface stationary points associated to the optimised structures. The time dependent density functional theory (TD-DFT)^{16d-f} allowed the computation of excitation energies, oscillator strengths and excited state compositions in terms of mono-electronic excitations between occupied and virtual orbitals. The weight of the mono-electronic excitation has been reported as the square of the coefficient of the Slater determinant associated to the mono-electronic excitation.

Acknowledgements

This research was supported by the Italian Ministero dell'Istruzione, dell'Università e della Ricerca (MIUR) through FIRB and the Centro di Eccellenza CEMIF.CAL grants. F. L. and M. A. thank PRIN 2002, CIPE CLUSTER 14 SP 5 and CIPE CLUSTER 26 SP 8 for financial support. M. A. thanks Consorzio INSTM for the contribution to his fellowship.

References

- (a) A. Curioni, M. Boero and W. Andreoni, *Chem. Phys. Lett.*, 1998, **294**, 263; (b) A. Curioni, W. Andreoni, R. Treusch, F. J. Himpsen, E. Haskal, P. Seidler, C. Heske, S. Kakar, T. van Buuren and L. J. Terminello, *Appl. Phys. Lett.*, 1998, **72**, 1575; (c) M. Amati and F. Lejl, *Chem. Phys. Lett.*, 2002, **358**, 144; (d) M. Amati and F. Lejl, *Chem. Phys. Lett.*, 2002, **63**, 451; (e) M. Amati and F. Lejl, *J. Phys. Chem. A*,

- 2003, **107**, 2560; (f) A. Curioni and W. Andreoni, *J. Am. Chem. Soc.*, 1999, **121**, 8216; (g) M. D. Halls and H. B. Schlegel, *Chem. Mater.*, 2001, **13**, 2632.
- 2 (a) C. W. Tang and S. A. VanSlyke, *Appl. Phys. Lett.*, 1987, **51**, 913; (b) P. E. Burrows, Z. Shen, V. Bulovic, D. M. McCarty, S. R. Forrest, J. A. Cronin and M. E. Thompson, *J. Appl. Phys.*, 1996, **79**, 7991; (c) W. Stampor, J. Kalinowski, G. Marconi, P. Di Marco, V. Fattori and G. Giro, *Chem. Phys. Lett.*, 1998, **183**, 373; (d) R. Treusch, F. J. Himpsel, S. Kakar, L. J. Terminello, C. Heske, T. van Buuren, V. V. Dinh, H. W. Lee, K. Pakbaz, G. Fox and I. Jimenez, *J. Appl. Phys.*, 1999, **86**, 88; (e) B. J. Chen, W. Y. Lai, Z. Q. Gao, C. S. Lee, S. T. Lee and W. A. Gambling, *Appl. Phys. Lett.*, 1999, **75**, 4010; (f) D. Ma, G. Wang, Y. Hu, T. Zhang, L. Wang, X. Jing, F. Wang, C. S. Lee and S. T. Lee, *Appl. Phys. Lett.*, 2003, **82**, 1296.
- 3 (a) C. W. Tang, S. A. VanSlyke and C. H. Chen, *J. Appl. Phys.*, 1989, **65**, 3610; (b) Y. Hamada, H. Kanno, T. Tsujioka, H. Takahashi and T. Usuki, *Appl. Phys. Lett.*, 1999, **75**, 1682; (c) K. Katsumura and Y. Shirota, *Adv. Mater.*, 1998, **10**, 223; (d) Y. Hamada, T. Sano, H. Fujii, Y. Nishio, H. Takahashi and K. Shibata, *Appl. Phys. Lett.*, 1997, **71**, 3338; (e) D. J. Fatemi, H. Murata, C. D. Merritt and Z. H. Kafafi, *Synth. Met.*, 1997, **85**, 1225; (f) Z.-I. Zhang, X.-Y. Jiang, S.-H. Xu, T. Nagatomo and O. Omoto, *Synth. Met.*, 1997, **91**, 131; (g) J. Shi and C. W. Tang, *Appl. Phys. Lett.*, 1997, **70**, 1665; (h) M. A. Baldo, D. F. O'Brien, A. Shoustikov, S. Sibley, M. E. Thompson and S. R. Forrest, *Nature*, 1998, **395**, 151; (i) G. Ponterini, N. Sermone, M. A. Bergkamp and T. L. Netzel, *J. Am. Chem. Soc.*, 1983, **105**, 4639.
- 4 G. Giro, M. Cocchi, P. Di Marco, V. Fattori, P. Dembeck and S. Rizzoli, *Synth. Met.*, 2001, **123**, 529.
- 5 (a) C. H. Chen and J. M. Shi, *Coord. Chem. Rev.*, 1998, **171**, 161; (b) J. Kido and J. Endo, *Chem. Lett.*, 1997, 593.
- 6 T. A. Hopkins, K. Meerholz, S. Shaheen, M. L. Anderson, A. Schmidt, B. Kippelen, A. B. Padias, H. K. Hall, N. Peyghambarian and R. Armstrong, *Chem. Mater.*, 1996, **8**, 344.
- 7 (a) G. Wang, F. Liang, Z. Xie, G. Su, L. Wang, X. Jing and F. Wang, *Synth. Met.*, 2002, **131**, 1; (b) Y. Qiu, Y. Shao, D. Zhang and X. Hong, *Jpn. J. Appl. Phys.*, 2000, **39**, 1151; (c) L. M. Leung, W. Y. Lo, S. K. Lo, K. M. Lee and W. K. Choi, *J. Am. Chem. Soc.*, 2000, **122**, 5640; (d) X. T. Tao, H. Suzuki, T. Wada, S. Miyata and H. Sasabe, *J. Am. Chem. Soc.*, 1999, **121**, 9447.
- 8 (a) S. A. VanSlyke, P. S. Bryan and F. V. Lovecchio, *US Pat.*, 5,150,006, 1992; (b) P. S. Bryan, F. V. Lovecchio and S. A. VanSlyke, *US Pat.*, 5,141,671, 1992; (c) P. Moore, S. A. VanSlyke and H. J. Gysling, *US Pat.*, 5,484,922, 1996.
- 9 I. S. Touloukhonova, I. A. Guzei, M. Kavana and R. West, *Main Group Met. Chem.*, 2002, **25**, 489.
- 10 K. Nakamaru, *Bull. Chem. Soc. Jpn.*, 1982, **55**, 2967.
- 11 (a) V. V. N. Ravi Kishore, K. L. Narasimhan and N. Periasamy, *Phys. Chem. Chem. Phys.*, 2003, **5**, 1386; (b) V. V. N. Ravi Kishore, A. Aziz, K. L. Narasimhan, N. Periasamy, P. S. Meenakshi and S. Wategaonkar, *Synth. Met.*, 2002, **126**, 199.
- 12 M. Kasha, *Discuss. Faraday Soc.*, 1950, **9**, 14.
- 13 A. Meyers, C. South and M. Weck, *Chem. Commun.*, 2004, 1176.
- 14 M. La Deda, M. Ghedini, I. Aiello and I. De Franco, *Inorg. Chem. Commun.*, 2004, **7**, 1273.
- 15 La Deda, A. Grisolia, I. Aiello, A. Crispini, M. Ghedini, S. Belviso, M. Amati and F. Lejl, *Dalton Trans.*, 2004, 2424.
- 16 (a) M. J. Frisch, G. W. Trucks, H. B. Schlegel, G. E. Scuseria, M. A. Robb, J. R. Cheeseman, V. G. Zakrzewski, J. A. Montgomery, Jr., R. E. Stratmann, J. C. Burant, S. Dapprich, J. M. Millam, A. D. Daniels, K. N. Kudin, M. C. Strain, O. Farkas, J. Tomasi, V. Barone, M. Cossi, R. Cammi, B. Mennucci, C. Pomelli, C. Adamo, S. Clifford, J. Ochterski, G. A. Petersson, P. Y. Ayala, Q. Cui, K. Morokuma, P. Salvador, J. J. Dannenberg, D. K. Malick, A. D. Rabuck, K. Raghavachari, J. B. Foresman, J. Cioslowski, J. V. Ortiz, A. G. Baboul, B. B. Stefanov, G. Liu, A. Liashenko, P. Piskorz, I. Komaromi, R. Gomperts, R. L. Martin, D. J. Fox, T. Keith, M. A. Al-Laham, C. Y. Peng, A. Nanayakkara, M. Challacombe, P. M. W. Gill, B. G. Johnson, W. Chen, M. W. Wong, J. L. Andres, C. Gonzalez, M. Head-Gordon, E. S. Replogle and J. A. Pople, *GAUSSIAN 98 (Revision A.11)*, Gaussian, Inc., Pittsburgh, PA, 2001; (b) R. G. Parr and W. Yang, *Density Functional Theory of Atoms and Molecules*, Oxford University Press, Oxford, 1989; (c) A. D. Becke, *J. Chem. Phys.*, 1993, **98**, 5648; (d) M. Casida, Time dependent density functional response theory for molecules in *Recent Advances in Density Functional Methods*, ed. D. P. Chong, World Scientific, Singapore, 1995, vol. 1, p. 155; (e) M. E. Casida, C. Jamorski, K. C. Casida and D. Salahub, *J. Chem. Phys.*, 1998, **108**, 4439; (f) R. E. Startmann and G. E. Scuseria, *J. Chem. Phys.*, 1998, **109**, 6218.